JOURNAL OF EXPERIMENTAL AND THEORETICAL PHYSICS, 2024, Vol. 165, No. 2, pp. 223–239

ORDER, DISORDER, AND PHASE TRANSITION IN CONDENSED MEDIA

PHASE DISTRIBUTION IN 1D LOCALIZATION AND PHASE TRANSITIONS IN SINGLE-MODE WAVEGUIDES

© 2024 I.M. Suslov

Kapitza Institute for Physical Problems, 119334 Moscow, Russia

e-mail: suslov@kapitza.ras.ru

Received May 31, 2023

Revised August 03, 2023

Accepted September 18, 2023

Abstract. Localization of electrons in 1D disordered systems is usually described in the random phase approximation, when distributions of phases φ and θ, entering the transfer matrix, are considered as uniform. In the general case, the random phase approximation is violated, and the evolution equations (when the system length L is increased) contain three independent variables, i.e. the Landauer resistance ρ and the combined phases $\psi = \theta - \varphi$ and $\chi = \theta + \varphi$. The phase χ does not affect the evolution of ρ and was not considered in previous papers. The distribution of the phase ψ is found to exhibit an unusual phase transition at the point $\mathcal{E}_0$ when changing the electron energy $\mathcal{E}$, which manifests itself in the appearance of the imaginary part of ψ. The resistance distribution $P(\rho)$ has no singularity at the point $\mathcal{E}_0$, and the transition looks unobservable in the electron disordered systems. However, the theory of 1D localization is immediately applicable to propagation of waves in single-mode optical waveguides. The optical methods are more efficient and provide possibility to measure phases ψ and χ. On the one hand, it makes observable the phase transition in the distribution $P(\psi)$, which can be considered as a "trace" of the mobility edge remaining in 1D systems. On the other hand, observability of the phase χ makes actual derivation of its evolution equation, which is presented below. Relaxation of the distribution $P(\chi)$ to the limiting distribution $P_\infty(\chi)$ at $L \to \infty$ is described by two exponents, whose exponentials have jumps of the second derivative, when the energy $\mathcal{E}$ is changed.

Keywords: *disordered systems*, *Landauer resistance*, *phase distribution*, *Lyapunov exponents*

DOI: 10.31857/S00444510240209e1

1. INTRODUCTION

Electron localization in one-dimensional disordered systems can be described by a transfer matrix T, which relates the wave amplitudes on the left ($Ae^{ikx} + Be^{-ikx}$) and right ($Ce^{ikx} + De^{-ikx}$) of the scatterer,

$$\begin{pmatrix} A \\ B \end{pmatrix} = T \begin{pmatrix} C \\ D \end{pmatrix}, \tag{1}$$

and in the presence of time-reversal invariance admits parameterization [1]:

$$T = \begin{pmatrix} 1/t & -r/t \\ -r^*/t^* & 1/t^* \end{pmatrix} = \begin{pmatrix} \sqrt{\rho+1}\, e^{i\varphi} & \sqrt{\rho}\, e^{i\theta} \\ \sqrt{\rho}\, e^{-i\theta} & \sqrt{\rho+1}\, e^{-i\varphi} \end{pmatrix}, \tag{2}$$

where t and r are the transmission and reflection amplitudes and $\rho = |r/t|^2$ is the dimensionless Landauer resistance [2]. When the scatterers are arranged in series, their transfer matrices are multiplied. For a weak scatterer, the matrix T is close to the unit one, which allows us to derive differential evolution equations (when the system length L changes) for its parameters.

Usually, such equations are derived in the random phase approximation, where the distributions of φ and θ are assumed to be homogeneous [3-8]. Such approximation works well for weak disorder in depth of the allowed zone, which is usually assumed in theoretical works (see references in [9-11]); fluctuation states in the forbidden band are discussed relatively rarely and only at the level of wave functions [12-14]. A systematic analysis shows that the random phase approximation is strongly violated near the initial band edge and in the forbidden band of an ideal crystal [15]. In the general

case, the evolution equations are written in terms of the Landauer resistance ρ and the combined phases (Section 2)

$$\psi = \theta - \varphi, \qquad \chi = \theta + \varphi. \tag{3}$$

The χ phase does not affect the evolution of ρ and is not of interest for condensed state physics; therefore, it was not discussed in previous papers [15-17]. Optical measurements (see below) allow us to study the distribution of the χ phase, which makes its theoretical study relevant.

The full evolution equation for the distribution $P(\rho, \psi, x)$ *is* derived in the Appendix. In fact, it has no practical significance: only its general structure, which provides the separation of variables, is essential (Section 2). The factorization $P(\rho, \psi, x) = P(\rho, \psi)P(\chi)$ is valid for arbitrary system length L, which allows us to restrict ourselves to the equations for $P(\rho, \psi)$ and $P(\chi)$. At large L the factorization $P(\rho, \psi) = P(\rho)P(\psi)$ arises, leading to the closed equation for $P(\rho)$ and the equation for the stationary distribution $P(\psi)$.

The stationary phase distribution ψ was studied in [16, 17]; in the depth of the disordered system, it experiences a peculiar phase transition at the point $\mathcal{E}_0$ at a change in the electron energy $\mathcal{E}$ [17], consisting in the appearance of the imaginary part of ψ (Section 3). In this case, the resistance distribution $P(\rho)$ has no singularity at the point $\mathcal{E}_0$, and the transition looks unobservable in the framework of condensed state physics.

The evolution equation for $P(\chi)$ is derived in Section 4: it has the form of an ordinary diffusion equation in which the diffusion coefficient and the drift velocity depend exponentially on L. The corresponding exponentials have singularities at changing $\mathcal{E}$, consisting in a jump of the second derivative (Sec. 5). Such phase transitions are also unobservable for electron disordered systems.

However, the approach used in [15-17] is directly applicable to describe the scattering of waves propagating in single-mode waveguides (Section 6.1). Existing optical methods (heterodyne approach, near-field microscopy, etc.) are efficient enough to measure the distribution of all parameters ρ, ψ, χ inside the waveguide[1] (Sect. 6.3). This extends the observable aspects of the one-dimensional localization theory and makes possible its deep experimental verification. In particular, phase transitions in the distributions of $P(\psi)$ and $P(\chi)$ become observable (Sects. 6.2, 6.3). Possible measurement schemes are discussed in Sect. 6.4.

A summary of the issues discussed is contained in the author's note with S.I. Bozhevolny [18].

2.GENERAL STRUCTURE OF THE EVOLUTION EQUATIONS

The most general evolution equation describes the change of the joint distribution function $P(p, \psi, \chi)$ with increasing system length L and has the following structure (see Appendix):

$$\frac{\partial P}{\partial L} = \left\{\hat{L}_{\rho,\psi} P\right\}'_{\rho} + \left\{\hat{M}_{\rho,\psi} P\right\}'_{\psi} + \left\{\hat{K}_{\rho,\psi,\chi} P\right\}'_{\chi}, \tag{4}$$

where $\hat{L}$, $\hat{M}$, $\hat{K}$ are some operators depending on the specified variables. The right part is the sum of full derivatives, which provides the conservation of probability. As discussed in [17, 19], the conditions for separation of variables in diffusion-type equations turn out to be weaker than for the eigenvalue problem. The independence of operators $\hat{L}$ and $\hat{M}$ from χ provides factorization $P(\rho,\psi,\chi) = P(\rho,\psi)P(\chi)$, where $P(\rho,\psi)$ and $P(\chi)$ are defined by equations

$$\frac{\partial P(\rho,\psi)}{\partial L} = \left\{\hat{L}_{\rho,\psi} P(\rho,\psi)\right\}'_{\rho} + \left\{\hat{M}_{\rho,\psi} P(\rho,\psi)\right\}'_{\psi} \tag{5}$$

and

$$\frac{\partial P(\chi)}{\partial L} = \left\{\hat{\mathcal{K}}_{\chi} P(\chi)\right\}'_{\chi}, \tag{6}$$

$$\hat{\mathcal{K}}_{\chi} = \int \hat{K}_{\rho,\psi,\chi} P(\rho,\psi) d\rho d\psi.$$

The specific form of equation (5) is given in [16, 17], and equation (6) is derived in Sect. 4. In the limit of large L, when typical values of ρ are large, the operator $\hat{M}_{\rho,\psi}$ becomes independent of ρ; then the solution of equation (5) is factorized, $P(\rho,\psi) = P(\rho)P(\psi)$, where for $P(\rho)$ and $P(\psi)$ the following equations are true

$$\frac{\partial P(\psi)}{\partial L} = \left\{\hat{M}_{\psi} P(\psi)\right\}'_{\psi}, \tag{7}$$

$$\frac{\partial P(\rho)}{\partial L} = \left\{\hat{\mathcal{L}}_{\rho} P(\rho)\right\}'_{\rho}, \quad \hat{\mathcal{L}}_{\rho} = \int \hat{L}_{\rho,\psi} P(\psi) d\psi. \tag{8}$$

[1] Of course, in this case the parameter p no longer has the sense of the Landauer resistance, but determines the amplitudes of the transmitted and reflected waves (Section 6.2).

The equation (7) ensures the existence of a stationary distribution of phase ψ. The equation (8) for $P(\rho)$ has the form [15]

$$\frac{\partial P(\rho)}{\partial L} = D\frac{\partial}{\partial \rho}\left[-\gamma(1+2\rho)P(\rho) + \rho(1+\rho)\frac{\partial P(\rho)}{\partial \rho}\right] \quad (9)$$

and at large L leads to a lognormal distribution

$$P(\rho) = \frac{1}{\rho\sqrt{4\pi DL}}\exp\left\{-\frac{[\ln\rho - \nu L]^2}{4DL}\right\}, \quad (10)$$

where $\nu = (2\gamma + 1)D$ The typical value of ρ grows exponentially with length L, which is an observable manifestation of the localization of states in one-dimensional systems. In the random phase approximation, the parameter γ is zero, and equations (9), (10) coincide with the results of [3-8]. The dependences of the parameters γ, D, ν on the reduced energy $\tilde{\mathcal{E}} = \mathcal{E}/W^{4/3}$, obtained on the basis of the analysis of moments for distribution of the transfer matrix elements [15], are shown in Fig. 1; here $\mathcal{E}$ is the energy counted from the initial band edge, and W is the amplitude of the random potential. All energies are measured in units of the hopping integral for the one-dimensional Anderson model, which is of the order of the initial band width. The violation of the random phase approximation is obvious.

It is clear from the above that the explicit form of equation (4) is of no practical importance, but only its general structure is essential. At arbitrary L it decomposes into two equations (5) and (6), and at large L – into three equations (6), (7), (8). It is also clear that the choice of independent variables ρ, ψ, χ is objective.

3. PHASE TRANSITION IN P(ψ) DISTRIBUTION

The meaning of the phase transition in the ψ distribution is that the distinction between the allowed and forbidden bands is preserved (in some sense) in the presence of a random potential, although the singularity of the density of states is smoothed out. This is reminiscent of the well-known argument by Mott [20] that the role of the allowed band edge comes to the mobility edge. In the one-dimensional case there is no mobility edge, but some "trace" of it remains. The fact is that in the allowed band ($\mathcal{E} > 0$) the trial scatterer is described by the transfer matrix (2), and in the forbidden zone ($\mathcal{E} < 0$) – by the pseudo-transfer matrix $\mathcal{T}$ [15] linking the coefficients at increasing and decreasing exponentials on the left ($Ae^{\kappa x} + Be^{-\kappa x}$) and right ($Ce^{\kappa x} + De^{-\kappa x}$) of the scatterer. In the simplest case, the matrix $\mathcal{T}$ is real and corresponds to the purely imaginary values of the phases θ and φ in formula (2). Let us compare the

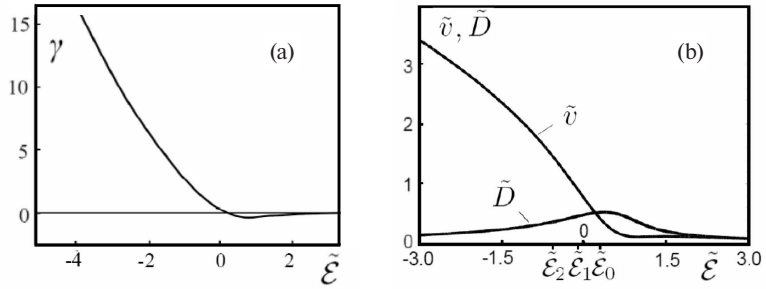

Fig. 1. Dependences of the parameters γ, $\tilde{v} = v / W^{2/3}$ and $\tilde{D} = D / W^{2/3}$ on the reduced energy $\tilde{\mathcal{E}} = \mathcal{E}/W^{4/3}$ obtained on the basis of the analysis of moments for the transfer matrix elements [15]. These moments are regular functions of energy, which ensures the regularity of the reduced dependences. The smallness of the parameter γ and the equality υ = D, which take place in the random phase approximation, are realized only in the depth of the allowed band. The points $\tilde{\mathcal{E}}_0$, $\tilde{\mathcal{E}}_1$, $\tilde{\mathcal{E}}_2$ correspond to the phase transitions discussed in Sects. 3 and 5.

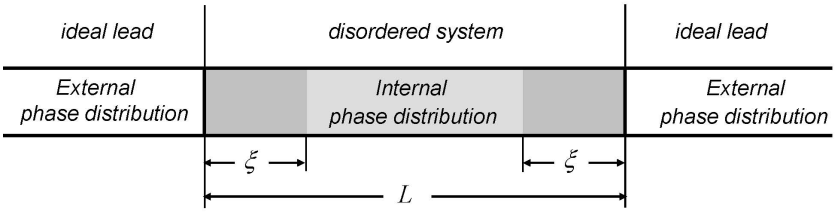

Fig. 2. External and internal phase distribution.

situation at $\mathcal{E} > 0$ and $\mathcal{E} < 0$: at a sufficient separation in energy the difference between the two types of matrices can be made as large as desired, and it cannot be overcome by adding weak disorder to the system. Therefore, the boundary between true and pseudo-transfer matrices can only shift, but cannot disappear[2]. In fact, this manifests itself in the appearance of the imaginary part of the ψ phase at energies $\mathcal{E} < \mathcal{E}_0$ [17].

The formal statements of [17] are summarized as follows. First of all, it is necessary to distinguish between "external" and "internal" phase distributions (Fig. 2). The internal distribution arises in the depth of a sufficiently long disordered system and does not depend on the boundary conditions. When considering the system from the side of ideal contacts, the "external" phase distribution, determined by boundary conditions, is observed; namely these phases appear in the transfer matrix. The influence of the interfaces is significant on a scale of the order of the localization length ξ, which defines a transition region in which the internal phase distribution is gradually transformed to the external one. In the limit of large L, the distribution $P(\rho)$ *is* determined by the internal phase distribution, which ensures its independence from the boundary conditions: the latter can be asserted at the formal level [15, 17]. However, it is the external phase distribution that enter the evolution equations, and it is necessary to understand why this does not affect the limiting distribution $P(\rho)$. The second question, related to the first one, is as follows: how can the internal phase distribution be found if it is not present in the equations?

The questions posed are resolved as follows. Phase ψ turns out to be a "bad" variable, and the "correct" variable is

$$w = -\cot\psi / 2. \tag{11}$$

The shape of the stationary distribution $P(w)$ is determined by the internal properties of the system and does not depend on the boundary conditions. Changes in the boundary conditions lead to three effects: the scale transformation $w \to sw$ and translations $w \to w + w_0$ and $\psi \to \psi + \psi_0$. The corresponding change in the distribution $P(\psi)$ is easily predictable [17] and can be observed in the external phase distribution. The evolution equations are invariant with respect to the translation $\psi \to \psi + \psi_0$ and the inner phase distribution can be discussed under some fixed choice of the origin. The invariance of the limiting distribution $P(\rho)$ with respect to the transformations $w \to sw$ and $w \to w + w_0$ is realized dynamically. Similar to the aperiodic oscillations of $P(\rho)$ [21,22], in the region $L \lesssim \xi$ the scale factor s and the translational shift w_0 experience oscillations as L changes, which decay when $L \to \infty$. As a result, s and w_0 tend to some "correct" values, which provide the correct values of D and v in the limiting distribution (10). The specified "correct" values[3] correspond to the intrinsic phase distribution and the latter can be found by returning to the variable ψ. It turns out that at $\mathcal{E} < \mathcal{E}_0$ the translational shift w_0 becomes complex-valued indicated the appearance of the imaginary part of the phase ψ. This change has a qualitative character, indicating the existence of a phase transition.

The point $\mathcal{E}_0$ is not singular for the resistance of the system ρ, so that the singular for distribution function $P(\rho)$ passes through it in a completely smooth way (Fig. 1 *b*). Therefore, in the framework of condensed state physics, the described phase transition looks unobservable. However, in optics it has observable manifestations in the form of root singularities in the frequency dependences (Sect. 6.2, 6.3).

4. EVOLUTION EQUATION FOR P(χ)

According to [17]. the change of the transfer matrix $T^{(n)}$ under increasing the number of scatterers n is determined by the recurrence relation

$$T^{(n+1)} = T^{(n)} T_\delta T_{\varepsilon_n}, \tag{12}$$

[2] Of course, one can object that in the presence of a random potential, spatial homogeneity is violated, and the shift of this boundary will depend on the position of the sample scatterer, leading to smearing of the phase transition. Physically, this is exactly what happens, ensuring the regularity of the Landauer resistivity ρ. However, the indicated band edge fluctuations are accounted for by spatial fluctuations in the phase ψ. The key point is that the distribution $P(\psi)$ is stationary and away from the system boundaries has spatial homogeneity: it is defined by some set of parameters that are coordinate independent. Therefore, for the distribution ψ in whole, the boundary between true and pseudo-transfer matrices is at a strictly defined energy. The stationary distribution $P(\psi)$ turns out to be the same both at a change of coordinate for a particular realization of the potential and at a change of the potential realization: in fact, this is ordinary ergodicity, since the coordinate x (Section 6) plays the role of time.

[3] The meaning of these values of s and w_0 is that the distribution $P(\psi)$ becomes stationary only at some "correct" boundary conditions, which are automatically formed at a distance of order ξ from the boundaries of the system. If the "correct" boundary conditions (defining s and w_0) are chosen at the boundary of the system with ideal contacts, the transition region of order ξ disappears and the stationary distribution is formed on very small scales, so that the distinction between the "outer" and "inner" phase distribution (Fig. 2) practically disappears. This provides a way to determine the "internal" phase distribution, which is not contained in the equations, through the "external" phase distribution, which enters the equations.

where the matrices $T^{(n)}$ and T_{ε_n} are statistically independent and T_δ is constant. It can be assumed that

$$T_{\varepsilon_n} = \begin{pmatrix} 1 - i\varepsilon_n & \varepsilon_n e^{i\gamma} \\ \varepsilon_n e^{-i\gamma} & 1 + i\varepsilon_n \end{pmatrix}, \tag{13}$$

$$T_\delta = \begin{pmatrix} A & B \\ B^* & A^* \end{pmatrix} = \\ = \begin{pmatrix} \sqrt{1+\Delta^2}\, e^{i\alpha} & \Delta e^{i\beta} \\ \Delta e^{-i\beta} & \sqrt{1+\Delta^2}\, e^{-i\alpha} \end{pmatrix}, \tag{14}$$

where ε_n is proportional to the amplitude of the n-th scatterer (and $\langle \varepsilon_n \rangle = 0$, $\langle \varepsilon_n^2 \rangle \equiv \varepsilon^2$), while T_δ is determined by a parameter δ proportional to the distance between the scatterers[4], and $\Delta \sim \alpha \sim \delta$ [17]. In the following we consider the limit

$$\delta \to 0, \quad \varepsilon \to 0, \quad \delta / \varepsilon^2 = \text{const} \tag{15}$$

and we keep the first order terms on δ and the second order terms on ε.

Taking the parameterization (2) for $T^{(n)}$ and denoting the parameters of the matrix $T^{(n+1)}$ as $\tilde\rho$, $\tilde\varphi$, $\tilde\theta$, we have

$$\sqrt{1+\tilde\rho}\, e^{i\tilde\varphi} = \sqrt{1+\rho}\, e^{i\varphi}(A + \varepsilon C) + \sqrt{\rho}\, e^{i\theta}(B^* + \varepsilon D^*), \tag{16}$$

$$\sqrt{\tilde\rho}\, e^{i\tilde\theta} = \sqrt{1+\rho}\, e^{i\varphi}(B + \varepsilon D) + \sqrt{\rho}\, e^{i\theta}(A^* + \varepsilon C^*),$$

where we set

$$C = Be^{-i\gamma} - iA, \qquad D = Ae^{i\gamma} + iB. \tag{17}$$

Squaring modulo one of equations (16), we obtain (omitting the index at ε_n)

$$\tilde\rho = \rho + K\sqrt{\rho(1+\rho)} + \varepsilon^2(1+2\rho), \tag{18}$$

where

$$K = 2\Delta\cos(\psi - \beta) + 2\varepsilon\cos(\psi - \gamma) - 2\varepsilon^2 \sin(\psi - \gamma). \tag{19}$$

By taking the product of the second equation (16) with the complex-conjugate of the first and eliminating $\tilde\rho$ using equation (18), we obtain the relation $\tilde\psi$ and ψ [17]

$$\tilde\psi = \psi + 2(\varepsilon - \alpha) + (R^2/2 - 1)\varepsilon^2 \sin 2(\psi - \gamma) - \\ -R\Big[\Delta\sin(\psi - \beta) + \varepsilon\sin(\psi - \gamma) + \varepsilon^2\cos(\psi - \gamma)\Big], \tag{20}$$

where

$$R = \frac{1+2\rho}{\sqrt{\rho(1+\rho)}}. \tag{21}$$

Relations (18) and (20) allow us to derive the evolution equation for $P(p, \psi)$ [17]. Now let us take the product of two equations (16)

$$\sqrt{\tilde\rho(1+\tilde\rho)}\, e^{i\tilde\chi - i\chi} = \sqrt{\rho(1+\rho)}(1 + 2\varepsilon^2) + \\ +\Delta\Big[e^{i(\beta-\psi)} + 2\rho\cos(\beta - \psi)\Big] + \\ +\varepsilon\Big[e^{i(\gamma-\psi)} + 2\rho\cos(\gamma - \psi)\Big] - \\ -\varepsilon^2\Big[ie^{i(\gamma-\psi)} - 2\rho\sin(\gamma - \psi)\Big] \tag{22}$$

and, excluding $\tilde\rho$, we obtain

$$\tilde\chi = \chi - f(\rho, \psi),$$

$$f(\rho,\psi) = \\ = \frac{\Delta\sin(\psi - \beta) + \varepsilon\sin(\psi - \gamma) + \varepsilon^2\cos(\psi - \gamma)}{\sqrt{\rho(1+\rho)}} - \\ - \frac{\varepsilon^2(1+2\rho)\sin 2(\psi - \gamma)}{2\rho(1+\rho)}. \tag{23}$$

Composing the evolution equation for $P(\chi)$,

$$P_{n+1}(\tilde\chi) = \int \delta\big(\tilde\chi - \chi + f(\rho,\psi)\big) P_n(\chi) \times \\ \times P_n(\rho,\psi) P_n(\varepsilon) d\chi\, d\rho\, d\psi\, d\varepsilon, \tag{24}$$

and performing trivial integration over χ, we have

$$P_{n+1}(\chi) = \Big\langle P_n\big(\chi + f(\rho,\psi)\big)\Big\rangle, \tag{25}$$

where ρ, ψ, ϵ are averaged over ρ, ψ, ε. Expanding the right-hand side over small quantity $f(\rho, \psi)$, one has

$$P_{n+1}(\chi) - P_n(\chi) = \\ = \Big\langle f(\rho,\psi)\Big\rangle \frac{dP_n}{d\chi} + \frac{1}{2}\Big\langle f(\rho,\psi)^2\Big\rangle \frac{d^2 P_n}{d\chi^2}, \tag{26}$$

which leads to the required equation

$$\frac{\partial P}{\partial L} = -v^* P'_\chi + D^* P''_{\chi\chi}, \tag{27}$$

[4] T_δ is constant if the distance between the scatterers is the same. Thus, in the one-dimensional Anderson model, scatterers are located at each site of the lattice: in this case, the number of scatterers n coincides with the system length L in units of the lattice constant.

which has the form of an ordinary diffusion equation with variable coefficients

$$v^* = \left\langle \frac{-\Delta\sin(\psi-\beta)+\varepsilon^2\cos(\psi-\gamma)\left[R\sin(\psi-\gamma)-1\right]}{\sqrt{\rho(1+\rho)}} \right\rangle, \quad (28)$$
$$D = \left\langle \frac{\varepsilon^2\sin^2(\psi-\gamma)}{2\rho(1+\rho)} \right\rangle$$

which are determined by averages over the distribution $P(\rho, \psi)$.

5. PHASE TRANSITIONS IN P(χ) DISTRIBUTION

For large L, the typical values of ρ are large, and in (28) we can restrict ourselves to the main order on $1/\rho$. Moreover, the distribution $P(p, \psi)$ is factorized, and the averaging over ρ and ψ is independent:

$$v^* = \left\langle -\Delta\sin(\psi-\beta)-\varepsilon^2\cos(\psi-\gamma)+\varepsilon^2\sin 2(\psi-\gamma) \right\rangle \times \left\langle \rho^{-1} \right\rangle, \quad (29)$$
$$D^* = \frac{1}{2}\left\langle \varepsilon^2\sin^2(\psi-\gamma) \right\rangle \left\langle \rho^{-2} \right\rangle.$$

The moments $\left\langle \rho^m \right\rangle$ for the log-normal distribution (10) have exponential behavior

$$\left\langle \rho^m \right\rangle \propto \exp(\kappa_m L) \quad (30)$$

with exponents

$$\kappa_m = \begin{cases} vm + Dm^2, & m > -v/2D \\ -v^2/4D, & m < -v/2D \end{cases}. \quad (31a), (31b)$$

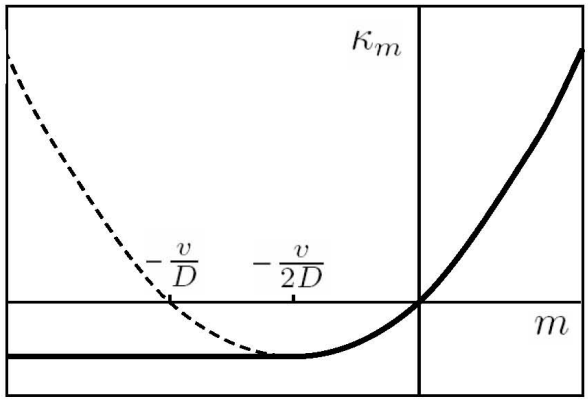

Fig. 3. Parameter κ_m in formula (30) as a function of m. The solid curve is realized, if restriction $\rho \gtrsim 1$ is accepted for the lognormal distribution (10), the dashed curve – in the absence of such a restriction

When computing $\left\langle \rho^m \right\rangle$ one must take into account that the lognormal distribution (10) is not valid for arbitrary ρ, but only for $\rho \gtrsim 1$; in the first case the result (31a) would be valid without restrictions[5] (Fig. 3).

The parameter κ_m is negative at $m < 0$, and it is convenient to put for clarity

$$\kappa_{-m} = -\tilde{\kappa}_m, \quad m > 0. \quad (32)$$

Due to the stationarity of the distribution $P(\psi)$, the average values for ψ in expressions (29) are reduced to constants, so that the equation for $P(\chi)$ takes the form

$$\frac{\partial P}{\partial L} = c_1 e^{-\tilde{\kappa}_1 L} P'_\chi + c_2 e^{-\tilde{\kappa}_2 L} P''_{\chi\chi} \quad (33)$$

and at large L is solved by iterative method:

$$P_L(\chi) =$$
$$= P_\infty(\chi) - \frac{c_1}{\tilde{\kappa}_1} e^{-\tilde{\kappa}_1 L} P'_\infty(\chi) - \frac{c_2}{\tilde{\kappa}_2} e^{-\tilde{\kappa}_2 L} P''_\infty(\chi), \quad (34)$$

where $P_\infty(\chi)$ is the limiting distribution at $L \to \infty$.

In Fig. 1 *b*, the points $\tilde{\mathcal{E}}_1$ and $\tilde{\mathcal{E}}_2$, corresponding to the conditions $v = 2D$ and $v = 4D$, are marked. If the lognormal distribution (10) were valid at arbitrary ρ, then at the point $\tilde{\mathcal{E}}_1$ there would be a striking phase transition associated with the change of the sign of $\tilde{\kappa}_2$ (point $-v/D$ in Fig. 3 at $\tilde{\mathcal{E}} = \tilde{\mathcal{E}}_1$ coincides with -2, so that $\tilde{\kappa}_2 > 0$ at $\tilde{\mathcal{E}} = \tilde{\mathcal{E}}_1$ and $\tilde{\kappa}_2 < 0$ at $\tilde{\mathcal{E}} = \tilde{\mathcal{E}}_1$): the effective diffusion coefficient in the equation (33) would grow with increasing L when $\tilde{\mathcal{E}} \geq \tilde{\mathcal{E}}_1$ and would decrease when $\tilde{\mathcal{E}} \leq \tilde{\mathcal{E}}_1$. At large L, the distribution of $P(\chi)$ would be homogeneous with high accuracy at $\tilde{\mathcal{E}} \geq \tilde{\mathcal{E}}_1$, while at $\tilde{\mathcal{E}} \leq \tilde{\mathcal{E}}_1$ some nontrivial distribution $P_\infty(\chi)$ would stabilize, which is determined by the early stage of evolution and lacking any universality.

[5] The integrand $\rho^m P(\rho)$ after substituting $x = \ln\rho$ has a Gaussian form, which is valid only at $x \gtrsim 1$. For $m > -v/2D$ the Gaussian function is strongly localized near a maximum located at large positive x, so that the restriction $x \gtrsim 1$ is insignificant for it. For $m < -v/2D$, the maximum of the Gaussian function goes to large negative x, and the integral is defined by its tail in the region $x \gtrsim 1$; the proportionality factor in (30) depends on the details of the distribution at $\rho \lesssim 1$, but the index κ_m does not depend on them.

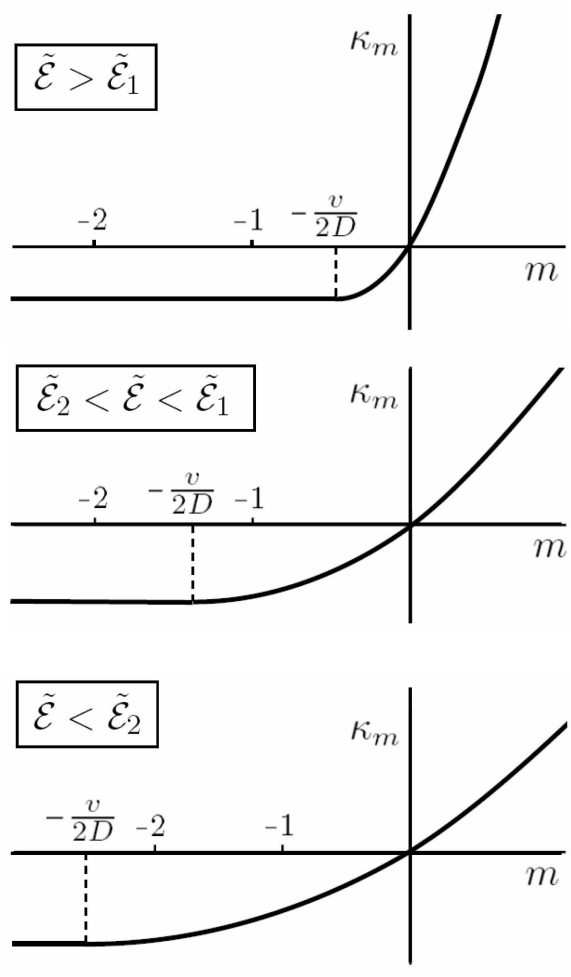

Fig. 4. Mutual location of the points $-v/2D$, -1 and -2 for $\tilde{\mathcal{E}} > \tilde{\mathcal{E}}_1$, $\tilde{\mathcal{E}}_2 < \tilde{\mathcal{E}} < \tilde{\mathcal{E}}_1$ and $\tilde{\mathcal{E}} < \tilde{\mathcal{E}}_2$

In the presence of the restriction $\rho \gtrsim 1$, such striking phase transition cannot be realized[6], but some singularity is preserved at the point $\tilde{\mathcal{E}}_1$; a similar singularity arises at the point $\tilde{\mathcal{E}}_2$. As is clear from Fig. 4, the point $-v/2D$, corresponding to matching of the parabola and the constant, at $\tilde{\mathcal{E}} > \tilde{\mathcal{E}}_1$, is to the right of the point -1 so that

$$\tilde{\kappa}_1 = \tilde{\kappa}_2 \quad for \quad \tilde{\mathcal{E}} > \tilde{\mathcal{E}}_1. \tag{35}$$

When $\tilde{\mathcal{E}}_2 < \tilde{\mathcal{E}} < \tilde{\mathcal{E}}_1$ the point $-v/2D$ is between the values -2 and -1, and when $\tilde{\mathcal{E}} < \tilde{\mathcal{E}}_2$ it is to the left of the point -2. It is not difficult to see that $\tilde{\kappa}_1$ has a jump of the second derivative at $\tilde{\mathcal{E}} = \tilde{\mathcal{E}}_1$, and $\tilde{\kappa}_2$ has a similar jump at $\tilde{\mathcal{E}} = \tilde{\mathcal{E}}_2$. Such jumps can be easily detected using equation (34): for this purpose, it is enough to find the limiting distribution $P_\infty(\chi)$ and to fit $P_L(\chi)$ by the dependence $P_\infty + aP'_\infty + bP''_\infty$: this is a linear fitting procedure implemented by standard programs [23]. The condition (15) corresponds to a large concentration of weak impurities: in this case, the coefficients in equation (27) change slowly, which leads to the formation for $P(\chi)$ of a Gaussian distribution with variable parameters[7]. It is determined by the first two moments, which significantly simplifies the processing.

Note that at point $\tilde{\mathcal{E}}_1$ there is a qualitative change consisting in violation of equality (35), whereas at point $\tilde{\mathcal{E}}_2$ there is simply a singularity.

6. MEASUREMENT CAPABILITIES IN SINGLE-MODE WAVEGUIDES

6.1. Analogy with optics

Localization of classical waves has been discussed in many papers [10,11, 24-30], which includes consideration of weak [25] and strong [26, 27] localization, absorption near the photon mobility threshold [24], near-field study of the intensity of optical modes in disordered waveguides [29], and many other aspects (see review [28]). The use of transfer matrices in this context has been discussed in [10, 11, 30]. As applied to optics, the corresponding analysis reduces to a few simple relations.

The propagation of an electromagnetic wave in a homogeneous dielectric medium is described by the wave equation

$$c^2\Delta\Psi - n^2\frac{\partial^2\Psi}{\partial t^2} = 0, \tag{36}$$

where Ψ is any component of an electric or a magnetic field. In a spatially inhomogeneous system, the refractive index n fluctuates with when change of coordinate x, i.e.

$$n^2(x) = n_0^2 + \delta n^2(x), \tag{37}$$

and for a monochromatic wave $\Psi \sim e^{iwt}$ leads to the equation

$$\tilde{c}^2\Delta\Psi + \left[\omega^2 + \omega^2\frac{\delta n^2(x)}{n_0^2}\right]\Psi = 0, \quad \tilde{c} = c/n_0, \tag{38}$$

[6] It is possible that under some special conditions the log-normal distribution may extend to the region of small ρ and this conclusion may be reconsidered.

[7] The above is true in the case of sufficiently strong localization of the distribution $P(\chi)$; in the general case it looks like a sum of Gaussian functions whose centers are separated by 2π, which provides 2π periodicity of the solution.

which structure corresponds to the Schrödinger equation for an electron with energy $\mathcal{E}$ and mass m in a random potential $V(x)$. In this case there is a correspondence

$$E \Leftrightarrow \omega^2, \frac{1}{2m} \Leftrightarrow \tilde{c}^2, V(x) \Leftrightarrow -\omega^2 \frac{\delta n^2(x)}{n_0^2}. \quad (39)$$

Some difference from condensed state physics is related to the dependence of $V(x)$ on ω (and hence on $\mathcal{E}$), which does not play an essential role if we restrict ourselves to a small range of frequencies in the continuous spectrum.

The spectrum of waves in a metal waveguide is analogous to the spectrum of electrons in a metal wire. In the latter case the transverse motion is quantized, which gives a set of discrete levels ε_s. Taking into account the longitudinal motion, these levels turn into one-dimensional bands with dispersion laws (Fig. 5 *a*)

$$\varepsilon_s(k) = \varepsilon_s + k^2/2m. \quad (40)$$

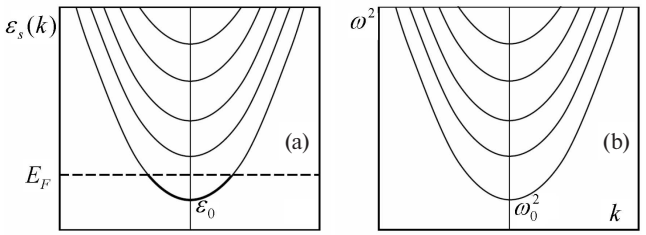

Fig. 5. Spectra of electrons in a metal wire (*a*) and waves in a metal waveguide (*b*)

To obtain a strictly one-dimensional system, the Fermi level should be small enough to fill only the lower band. In the presence of impurities, the lower boundary of the spectrum ε_0 is smeared out due to the appearance of fluctuation states at $\mathcal{E} < \varepsilon_0$. The dependencies in Fig. 1 correspond to the energy $\mathcal{E}$ counted from ε_0.

Similarly, in a metallic waveguide, quantization of the transverse motion gives a set of discrete frequencies ω_s, such that $\omega_s = \tilde{c}\kappa_s$, where $-\kappa_s^2$ is an eigenvalue of the two-dimensional Laplace operator with appropriate boundary conditions [31]. A zero eigenvalue is possible only when the cross section of the waveguide is multi-connected (as in a coaxial cable). For a singly connected cross section, the minimum value of ω_0 is finite [31], and taking into account the longitudinal motion we have the following spectrum branches (Fig. 5 *b*)

$$\omega_s^2(k) = \omega_s^2 + \tilde{c}^2 k^2. \quad (41)$$

In order to realize the single-mode regime, it is necessary to work near the lower bound of the spectrum ω_0. In the presence of disorder, the lower bound ω_0 is blurred by the appearance of fluctuation states. Thus, all the effects that take place in the electronic system when the Fermi level changes can be observed in a single-mode waveguide when the frequency ω changes in the vicinity of ω_0.

The spectrum in Fig. 5 *b* is valid for a metallic waveguide, which is a hollow metallic tube that can be filled with a non-absorbing dielectric. The latter case (dielectric waveguide with a metallic coating) is of primary interest for our purposes because of the possibility of introducing impurities that provide sufficiently strong elastic scattering. The thickness of the metal coating should be of the order of the skin layer depth to provide partial transparency to an electric field (Sect. 6.4). In a metallic waveguide, the transverse motion is confined to a potential well with infinite walls so that the multiplier ω^2 in (39) does not matter and the parameters κ_s are constants depending only on the shape of the waveguide cross section; accordingly, the spectrum in Fig. 5 *b* is strictly parabolic.

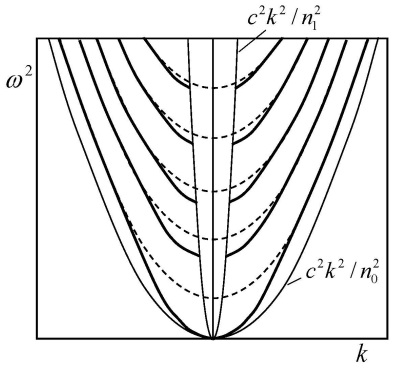

Fig. 6. Wave spectrum in a dielectric waveguide with refractive index n_0 inside the waveguide and n_1 in the surrounding space. At large ω, the spectrum is the same as in the metallic waveguide (the walls of the potential well are almost infinite); as ω decreases, deviations from the parabolic dependence shown by the dashed line occur. The restriction from below for the allowed values of the longitudinal momentum k arises due to the violation at small k of the conditions for total internal reflection. The disappearance of the boundary frequency ω_0 is due to the fact that the value of κ_0^2 is limited from above by the depth of the potential well proportional to ω^2.

In the absence of a metallic coating (purely dielectric waveguide), the transverse motion is limited by a potential well with finite walls, so the dependence of the effective potential $V(x)$ on frequency (see (39)) becomes significant. The parameters κ_s cease

to be constant and acquire dependence on ω, which leads to deviations from the parabolic dependence in the coordinates (ω^2, k). In particular, the value of κ_0^2 is limited by the depth of the potential well proportional to ω^2, which leads to the disappearance of the boundary frequency ω_0 (Fig. 6). In addition, there are restrictions from below on the allowed values of the longitudinal momentum k, due to the violation at small k of the conditions for total internal reflection. In the usual Schrödinger equation, the bound states in the potential well $V(x)$ lie in the energy interval $V_{\min} < E < V_\infty$, where $V_{\min}$ is the minimum value of the potential $V(x)$, and V_∞ is its limiting (constant) value at infinity. In a dielectric waveguide, the analogous condition is $n_1^2\omega^2 < c^2k^2 < n_0^2\omega^2$, where n_0 and n_1 are refractive indices inside the waveguide and in the surrounding space: as a result, the wave spectrum in the waveguide is bounded by two parabolas (Fig. 6). It is easy to see that in the case of a purely dielectric waveguide, the analogy with electronic systems is broken: everything that corresponds to the forbidden zone is missing, and some differences occur near the edge of the zone. However, the allowed band remains accessible for investigation[8]: in particular, the phase transition in the distribution $P(\psi)$ is in the allowed band (Fig. 1 *b*) and can be preserved in a dielectric waveguide (although this cannot be asserted at a formal level). Its preservation is likely if the disorder is strong enough and the expected transition falls in the region where the difference between the real spectrum and the parabolic spectrum is not too large.

6.2. Registration of phase transition in the distribution $P(\psi)$

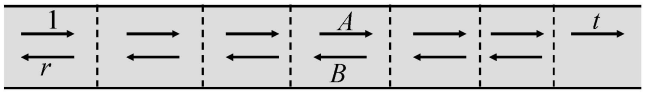

Fig. 7. Wave propagation in a waveguide with point scatterers.

Suppose a wave of unit amplitude is incident on the left side of the waveguide, which with amplitude t passes through the entire waveguide, and with amplitude r is reflected (Fig. 7). If there are point scatterers in the waveguide, partial reflection occurs at each of them. Therefore, at an arbitrary point x of the waveguide, we have a superposition of two waves traveling in a opposite directions; the electric field $E(x,t)$ is determined by its real part:

$$E(x,t) = \mathrm{Re}\left[Ae^{ikx+i\omega t} + Be^{-ikx+i\omega t} \right]. \qquad (42)$$

If the transfer matrix T *is* defined according to (1), (2), then the wave amplitudes in superposition (42) are determined by the relation

$$\begin{pmatrix} A \\ B \end{pmatrix} = T\begin{pmatrix} t \\ 0 \end{pmatrix} = \begin{pmatrix} |t|\sqrt{\rho+1}\,e^{i\varphi-i\varphi_0} \\ |t|\sqrt{\rho}\,e^{-i\theta-i\varphi_0} \end{pmatrix}, \qquad (43)$$

where ρ, ψ, θ depend on x and it is assumed $t = |t|e^{-i\varphi_0}$. If the amplitude $|t|$ is small enough, then the magnitude of ρ is large in almost the entire waveguide (except in the neighborhood of the right edge). Then $|A| \approx |B|$, and in this approximation (42) gives

$$\begin{aligned} E(x,t) &= \mathrm{Re}\left[\begin{matrix} |A|e^{ikx+i\omega t+i\varphi-i\varphi_0} + \\ +|B|e^{-ikx+i\omega t-i\theta-i\varphi_0} \end{matrix} \right] \approx \\ &\approx 2|A|\cos\left(kx+\chi/2\right)\cos\left(\omega t-\psi/2-\varphi_0\right), \end{aligned} \qquad (44)$$

so that the phase χ defines the coordinate dependence and the phase ψ – the time dependence. The phases ψ and χ remain constant between scatterers and change by a jump as they pass through the scatterer. At large impurity concentrations, their coordinate dependence becomes practically continuous and corresponds to random fluctuations on the scattering length scale.

Since the field $E(x, t)$ is measurable, both phases χ and ψ are theoretically observable. This is a fundamental difference from condensed state physics, where the superposition of waves refers to the wave function, and for the transition to observable quantities must be squared modulo: in this case the phase ψ is unobservable at all. However, the phase ψ becomes unobservable also in optics if only the average intensity is measured, i.e. if (44) is squared and averaged over time. It is not difficult to check that this conclusion holds also under the condition $|A| \neq |B|$.

Nevertheless, the appearance of the imaginary part ψ can be registered in this case as well. Assuming

$$\varphi = \varphi' + i\varphi'', \quad \theta = \theta' + i\theta'', \qquad (45)$$

we have for the amplitudes in the linear combination (42)

$$|A| = |t|\sqrt{\rho+1}\,e^{-\varphi''}, |B| = |t|\sqrt{\rho}\,e^{\theta''}. \qquad (46)$$

[8] For experiments, a purely dielectric waveguide has the advantage of no ohmic losses in the metal coating.

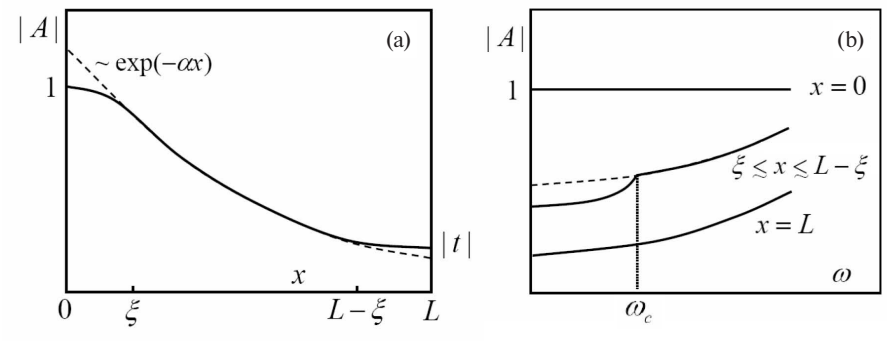

Fig. 8. (*a*) – Dependence of the amplitude A of the traveling wave on the coordinate x inside the waveguide. (*b*) – Dependence of |A| on the frequencies in the vicinity of the phase transition

The flux conservation requires[9] that the condition $|A|^2 = |B|^2 + |t|^2$ must be satisfied, which reduces to

$$(\rho + 1)e^{-\varphi''} = \rho e^{-\theta''} + 1 \tag{47}$$

and at large ρ gives $\theta'' = -\varphi''$. It is easy to see that the imaginary part is absent for the phase χ, but is admissible for phase ψ; thus $\psi'' = 2\theta'' = -2\varphi''$, and in particular

$$|A| = |t|\sqrt{\rho + 1}e^{\psi''/2}. \tag{48}$$

The critical behavior of the imaginary part ψ can be established from general considerations. Let there be an equation $F(x) = 0$, where the function $F(x)$ depends on some external parameter ε in a regular way. If two real roots become complex at the intersection of the point $\varepsilon = 0$, then at $\varepsilon = 0$ there is a multiple root $x = p$ in the neighborhood of which (assuming finiteness of the first derivative of ε) the equation has the form

$$(x - p)^2 - a\varepsilon = 0, \tag{49}$$

which at $a\varepsilon > 0$ gives the roots $p \pm \sqrt{a\varepsilon}$, and at $a\varepsilon < 0$ the roots $p \pm i\sqrt{|a\varepsilon|}$. Thus, the appearance of the imaginary part of x is related to the square root singularity. According to Sect. 3, the imaginary part ψ arises as a result of the selection of the parameters s and ω_0, providing the correct values of v and D in the lognormal distribution (10). Thus, s and ω_0 are determined by the solution of some equations, the numerical analysis of which shows [17] that the appearance of the imaginary part ω_0 is associated with the merging of two real roots and their subsequent transition to the complex plane[10]. Therefore, the above considerations are directly relevant: if the imaginary part ψ appears when $\omega < \omega_c$, then it has the behavior[11]

$$\psi'' \sim \sqrt{\omega_c - \omega}\,\Theta(\omega_c - \omega). \tag{50}$$

According to [17], the distribution $P(\rho)$ has no singularity at $\omega = \omega_c$ (Fig. 1 *b*). This applies to the value of ρ at any point in the waveguide, and in particular to its value at the full length of L, which is related to t by the relation $|t| = (1 + p)^{-1/2}$. Therefore, the singularity in (48) is entirely determined by the value of ψ'' and has a square root nature. Such singularities at the point $\mathcal{E}_0$ are visually distinguishable in Figures 8 and 11 of [17], although they are obtained as a result of numerical analysis.

The general picture appears as follows. The modulus A varies inside the waveguide basically according to the exponential law $|A| \sim e^{-ax}$, but there are deviations from it at a distance of order ξ from the edges of the system, related to the influence of boundary conditions (Fig. 8 *a*); thus $|A| = 1$ for $x = 0$ and $|A| = |t|$ for $x = L$. The latter value is related to ρ and is therefore regular for ω. However, far from the edges of the waveguide, the magnitude $|A|$ has a square root singularity (Fig. 8 *b*), which can be detected already in the average intensity measurement. Such a singularity is observable at a particular point in the system

[9] The scattering is assumed to be purely elastic. The inevitable ohmic losses in the metallic coating of the waveguide are assumed to be weak enough for localization effects to dominate. Sufficiently strong elastic scattering can in principle be ensured: so, in the case of optical fibers it is considered to be established that scattering on impurities is the main scattering for not too pure fibers [32].

[10] The second real root corresponds to a non-physical branch and therefore was not discussed in [17].

[11] Usually in the theory of phase transitions the square root behavior of the order parameter corresponds to the mean-field theory, whereas the accounting of fluctuations leads to the formation of a nontrivial critical index β smaller than 1/2. At present, we see no grounds for the realization of such scenario.

for a particular realization of the potential, since the transition from the true to the pseudo-transfer matrix occurs at an energy corresponding to the renormalized edge of the zone shifted by the random potential[12]. This shift varies from point to point (see footnote 2), but for the distribution function as a whole corresponds to a strictly defined energy. Therefore, the phase distribution moments also have a square root singularity (see the end of Section 6.3)

According to [17], the transition point $\mathcal{E}_0$ is located in the initial allowed band at a distance of the order of $W^{4/3}$ from the band edge (Fig. 1 *b*). Accordingly, in optics the critical point ω_c is greater than the boundary frequency ω_0, and the distance between them is determined by the degree of disorder.

6.3 Observability of phases ψ and χ

Measuring the time dependence at optical frequencies is generally not possible. However, the observability of the phase ψ can be ensured by using the heterodyne technique, when an auxiliary field $E_s(x,t)$ is added to the measured field, whose frequency is shifted by a small value Ω:

$$E + E_s = \mathrm{Re}\left\{\left|E\right|e^{i\omega t + i\varphi_E} + \left|E_s\right|e^{i(\omega+\Omega)t + i\varphi_s}\right\}. \quad (51)$$

Passing to the intensity and averaging fast oscillations over time, we have

$$\begin{aligned}\overline{2(E+E_s)^2} &= \left|E\right|^2 + \left|E_s\right|^2 + \\ &+ 2\left|E\right|\left|E_s\right|\cos\left(\Omega t + \varphi_s - \varphi_E\right),\end{aligned} \quad (52)$$

so that the phase φ_E enters in combination with Ωt, which provides the possibility of its measurement. For the field $E(x,t)$ corresponding to the result (44), we obtain

$$\begin{aligned}\overline{2\left(E+E_s\right)^2} &= \left\{4\left|A\right|^2\cos^2\left(kx+\chi/2\right) + \left|E_s\right|^2\right\} + \\ &+ 2\left|A\right|\cos\left(kx+\chi/2\right)\times \\ &\times 2\left|E_s\right|\cos\left(\Omega t + \psi/2 + \varphi_0 + \varphi_s\right),\end{aligned} \quad (53)$$

so that both phases χ and ψ turn out to be observable, and can be extracted from the experiment by the following treatment.

The stationary first term in the right-hand side of (53) and the time oscillating second term can be separated by Fourier analysis. The stationary contribution $|E_s|^2$ is easily separated because the minimum value of the first term in the curly bracket is zero. Since the cosine varies in a regular way and changes sign each time it passes through zero, the square root of the first term in curly brackets can be extracted to an insignificant common sign. As a result, two combinations are known separately

$$\left|A\right|\cos\left(kx+\chi/2\right) \text{ and } \left|E_s\right|\cos\left(\Omega t + \psi/2 + \varphi_0 + \varphi_s\right). \quad (54)$$

The multiplier $|E_s|$ in the second combination is determined from the time amplitude of the oscillations[13], and then the dependence of this combination on x can be assigned to the phase ψ.

The processing of the first combination in (54) is complicated by the fact that $|A(x)|$ does not strictly follow the exponential $\exp(-\alpha x)$ relation, but has significant fluctuations around it $E(x,t)$, being determined by the log-normal distribution the (10). The correct treatment appears as follows.

1. Determine k from the average oscillation period.

2. Find the values of χ at discrete points – maxima, minima, and zeros of the oscillatory dependence – by the deviation of their positions from the pure cosine. If the value of k is chosen correctly, the resulting values of χ will fluctuate near a constant level and will not grow systematically. This defines the data set for analyzing the distribution of χ.

3. Determine the values of $|A(x)|$ at the points of maxima and minima. This allows to accumulate statistics to check the log-normal distribution and to detect systematic deviations from the exponential dependence at the edges of the waveguide.

The observability of the phase ψ gives additional possibilities to register the phase transition in the distribution $P(\psi)$. If we pass from ψ to the variable w defined in (11), the moments of the distribution $P(w)$ (in particular $\langle w\rangle$) will have singularities $\sqrt{\omega-\omega_c}$ in the region $\omega > \omega_c$. The phase χ does not affect the evolution of the resistivity distribution and therefore has not been studied in [16, 17]. However, its observability in optics makes such studies relevant.

[12] In this case, the square root singularity can be obtained trivially from the behavior of the true and pseudo transfer matrix for a point scatterer as it approaches the edge of the initial band (see [15]), taking into account its fluctuation shift.

[13] Another way to reach the same result is to make measurements at several values of $\left|E_s\right|$ and fit the right-hand side of (53) by the dependence $\alpha + \beta\left|E_s\right| + \gamma\left|E_s\right|^2$.

6.4. Possible measurement schemes

Measurement of the electric field inside the waveguide is possible using a near-field scanning optical microscope [33-35]. There are two types of such a microscope – detecting and scattering: depending on this, two different measurement schemes are possible. The comparison of these two schemes leads to a combined variant in which the detection problem is reduced to atomic force [36, 37] or tunneling [38] microscopy.

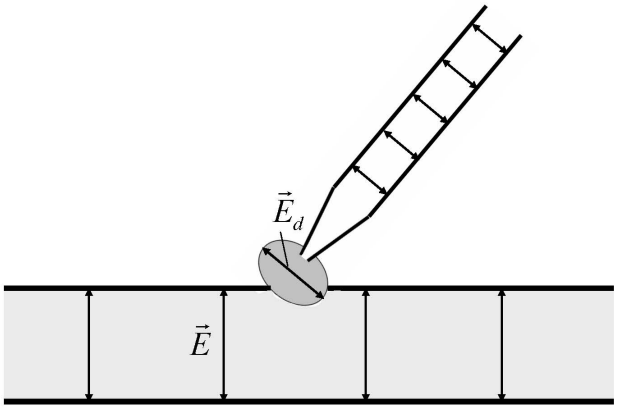

Fig. 9. Measurement of the field in a waveguide using a near-field scanning optical microscope.

Detecting regime. In this case, the optical microscope needle (a fragment of metal-coated optical fiber) is a waveguide with a constriction at the end and a hole of diameter d smaller than the wavelength (Fig. 9). The field created by it in the near zone can be represented as a "cloud" of finite volume $V_\mathrm{d} \sim d^3$ (see Fig. 4 in [35]), the electric field $\mathbf{E}_d$ in which is approximately constant and oriented parallel to the field inside the needle. Let the tip of the probe is approaching at some angle the surface of the given waveguide, so that some volume V of the "cloud" penetrates inside the waveguide (Fig. 9). If $\mathbf{E}$ is the electric field inside the waveguide, the energy change due to the penetration of the "cloud" is defined by the expression

$$\left[(\mathbf{E}+\mathbf{E}_d)^2-\mathbf{E}^2-\mathbf{E}_d^2\right]V=2\mathbf{E}\cdot\mathbf{E}_d V. \tag{55}$$

At small displacements of the needle x, the volume change is proportional to the displacement, $\delta V = S\mathrm{x}$, where S is the area of intersection of the "cloud" with the surface of the waveguide. Therefore, the force acting on the microscope needle is determined by expression (55) with V replaced by S and depends on the measured field. It can be converted into a displacement of the needle or a change in the voltage holding the needle in a constant position. In reality, the $\mathbf{E}_d$ field depends on the coordinates and instead of (55) we should write

$$\int 2\mathbf{E}\cdot\mathbf{E}_d(r)d^3r \tag{56}$$

with integration over the waveguide volume, which, as a result of a rough evaluation of the integral, returns to (55).

Considering that $E \sim E_d$ and introducing atomic units of field strength and force

$$E_0=\frac{e}{a^2}\sim 10^9 V/\mathrm{sm},\quad F_0=\frac{e^2}{a^2}\sim 10^{-2}\,\mathrm{dyn}, \tag{57}$$

we obtain an estimate of the force acting on the needle

$$F\sim F_0\left(\frac{E}{E_0}\right)^2\left(\frac{d}{a}\right)^2. \tag{58}$$

Since the hole size d is limited by the condition $d \lesssim \lambda \sim 10^4 a$, it can be assumed that

$$F\sim 10^6\left(\frac{E}{E_0}\right)^2 dyn. \tag{59}$$

The maximum field value is limited by the dielectric breakdown field of the order of 10^7 V/cm. If we take the value $F \sim 10^{-8}$ dyn, which is characteristic for tunneling microscopy [38], as the limit of sensitivity, there is a wide range of fields

$$10^{-7}E_0 \lesssim E \lesssim 10^{-2}E_0, \tag{60}$$

for which the outlined scheme is realistic.

If the field $\mathbf{E}_s$ with shifted frequency is used as $\mathbf{E}_d$ (see (51)), the force acting on the needle is determined by the quantity

$$\begin{gathered}F\sim S|A||E_s|\times\\ \times\cos\left(kx+\chi/2\right)\cos\left(\Omega t+\psi/2+\varphi_0+\varphi_s\right),\end{gathered} \tag{61}$$

whose treatment is even simpler than expression (53). Above, we did not take into account the presence of a semi-permeable metallic coating (Sect. 6.1) and the difference from unity of the dielectric constant inside the waveguide. Taking these factors into account leads to the addition in the right part of (61)

of an additive term of the order E_s^2, independent of the measured field and easily separable during processing.

The general scheme of measurements is presented as follows (Fig. 10). The beam from the laser is split into two parts, one of which is directed into the waveguide. The second part falls on an oscillating mirror, which leads to a frequency shift by Ω due to the Doppler effect. Since the velocity of the mirror is variable, it leads to a variable shift Ω. This problem can be solved by recording the time dependence at discrete points, equidistant of the harmonic one. Another possibility is to realize a saw-toothed regime of oscillations rather than a harmonic oscillation. From the mirror, the beam is directed into the microscope needle, at the end of which a field $\mathbf{E} + \mathbf{E}_s$ appears, which makes it possible to measure the coordinate dependence of the field $\mathbf{E}$ as a result of scanning the waveguide surface.

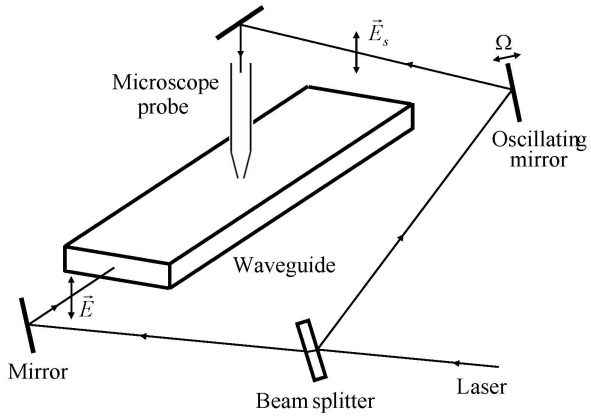

Fig. 10. General scheme of measurements in the detecting regime of a near-field optical microscope.

Scattering regime. In this case, the optical microscope needle is used not for immediate field detection, but only as a source of scattering[14]. A wave, propagating in the waveguide, penetrates beyond its boundaries due to the tunneling effect and can be scattered at the tip of the needle, located close to the waveguide surface. For sub-wavelength-sized probe tips, the scattering occurs in the Rayleigh regime, and the electric field in the scattered wave is proportional to the field $E(x, t)$ in the waveguide[15] at the scattering point x.

[14] It can be replaced by a tunneling microscope needle, which, in the presence of a metal coating (Section 6.1), allows all the advantages of scanning tunneling microscopy [38].

[15] In Rayleigh scattering, the field of the scattered wave in the main approximation is determined by the electric field of the incident wave and does not depend on the wave vector of the latter [31]. Therefore, the two waves entering the superposition (42) are scattered equally, and the total field of the scattered wave is proportional to the field in the waveguide.

The general scheme of measurements is as follows (Fig. 11). The beam from the laser is split into two parts, one of which is directed into the waveguide and scattered on the microscope needle. The scattered light is collected by a parabolic mirror and directed to a beam combiner. The second part of the laser beam falls on the oscillating mirror and acquires a shift frequency Ω due to the Doppler effect. From the mirror, the beam is directed to the beam combiner, where it is mixed with the first beam and directed to the photodiode for intensity measurement. The outlined scheme is practically realized in [39], where the missing experimental details can be found.

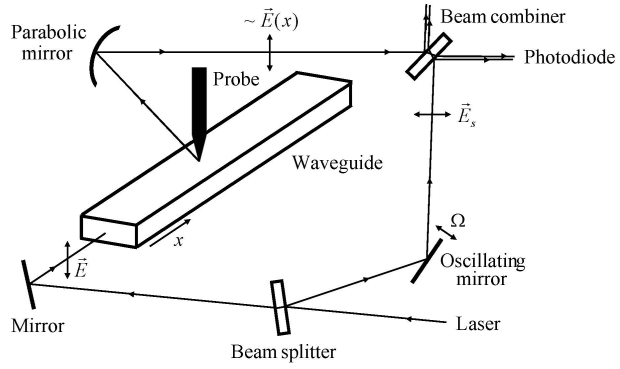

Fig. 11. Schematic of electric field measurements in the waveguide for the scattering mode of the near-field optical microscope.

The combined scheme differs from the scheme in Fig. 10 in that the second beam from the mirror does not go to the microscope needle, but is directed to the waveguide, shining through it in the transverse direction near the surface (Fig. 12). Since the field $\mathbf{E}$ due to the tunnel effect penetrates beyond the waveguide, there is a field $\mathbf{E} + \mathbf{E}_s$ near its surface, the energy of which changes as the microscope needle approaches the surface due to the dielectric polarizability of the needle. As a result, the force acting on the needle is proportional to the intensity of the field $\mathbf{E} + \mathbf{E}_s$, and the problem of its measurement is reduced to atomic force [36, 37] or tunnel [38] microscopy.

7. CONCLUSIONS

It has been shown above that all the results obtained for electrons in one-dimensional disordered systems are directly applicable to the scattering of waves propagating in single-mode waveguides. Modern optical methods make it possible to measure all parameters ρ, ψ, χ entering the transfer matrix. As a result, it becomes possible to observe a phase transition in the

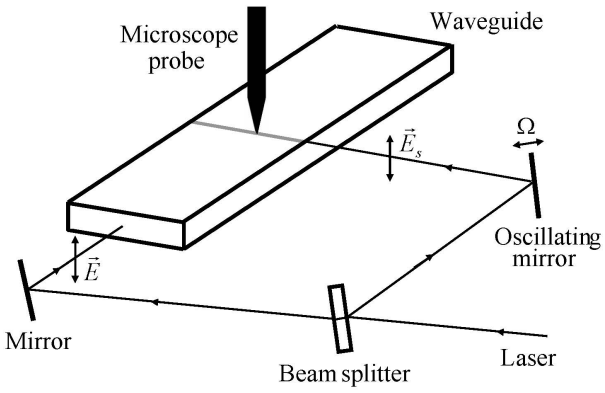

Fig. 12. Measuring the electric field in a waveguide using an atomic force or tunneling microscope.

phase distribution ψ, which looks unobservable in the context of condensed state physics.

The observability of the χ phase makes it relevant to derive an equation for the evolution of its distribution, which has not been studied in previous works. At large L, the distribution of χ has singularities consisting in jumps of the second derivative for the exponents describing the relaxation of $P_L(\chi)$ to the limit distribution $P_\infty(\chi)$.

As indicated above, one of the measurement schemes described in Sect. 6.4 was implemented in [39]. In contrast to the experiments [40, 41], where only the transmission matrix was measured, the approach proposed in [39] allows measuring the phase distribution inside the waveguide. However, the measurements performed in [39] are not related to light propagation in disordered systems, but only to the study of regular modes in homogeneous waveguides.

Essentially new experiments are required to verify the validity of the statements made in the present work. First of all, such experiments should use a tunable laser that allows changing the frequency of emission, and its frequency range should overlap the position of the expected phase transition. The latter requires establishing the most suitable waveguide configuration and dimensions. An efficient method for introducing a large concentration of impurities into the waveguide is required. A detailed analysis is needed to find the parameter region in which elastic scattering dominates absorption inside the waveguide and radiation losses through its walls. The latter problem is somewhat alleviated when a purely dielectric waveguide is used, but in this case, the analogy with electronic disordered systems becomes incomplete (Section 6.1).

We hope that the results will stimulate experimental research in this area and lead to a better understanding of localization effects in both electronic and optical systems.

ACKNOWLEDGMENTS

The author is grateful to S.I. Bozhevolny for discussion of the optical aspects of the paper.

APPENDIX

Equation of evolution for $P(\rho, \psi, \chi)$

The following derivation of the evolution equation differs from that in [16, 17]: it leads to longer calculations, but is more systematic, guaranteeing a result when its nature is not known in advance. The more compact way of derivation given in [16, 17] can be found only if there is some information about the structure of the result.

At the level of relations (18), (19), (20), (22), we can understand that the value of ψ enters the evolution equations in the form of two combinations $\psi - \gamma$ and $\psi - \beta$, so that by shifting $\psi \to \psi + \psi_0$ the parameter γ can be reduced to the value $-\pi/2$ corresponding to a sharp interface [17]; to simplify the formulas we will restrict ourselves to this case. Relations (12)–(14) at low order in δ give

$$\begin{aligned} T_{11}^{(n+1)} &= (1 + i\alpha - i\varepsilon_n)T_{11}^{(n)} + (\delta_1 - i\delta_2 + i\varepsilon_n)T_{12}^{(n)}, \\ T_{12}^{(n+1)} &= (\delta_1 + i\delta_2 - i\varepsilon_n)T_{11}^{(n)} + (1 - i\alpha + i\varepsilon_n)T_{12}^{(n)} \end{aligned} \tag{A.1}$$

and similar equations for $T_{21}^{(n)}$ and $T_{22}^{(n)}$, obtained by complex conjugation; here $\delta_1 = \Delta\cos\beta$, $\delta_2 = \Delta\sin\beta$. Assuming

$$T_{11}^{(n)} = x_n + iy_n, \quad T_{12}^{(n)} = z_n + iw_n, \tag{A.2}$$

we have

$$\begin{aligned} x_{n+1} &= x_n - (\alpha - \varepsilon_n)y_n + \delta_1 z_n + (\delta_2 - \varepsilon_n)w_n, \\ y_{n+1} &= (\alpha - \varepsilon_n)x_n + y_n - (\delta_2 - \varepsilon_n)z_n + \delta_1 w_n, \\ z_{n+1} &= \delta_1 x_n - (\delta_2 - \varepsilon_n)y_n + z_n + (\alpha - \varepsilon_n)w_n, \\ w_{n+1} &= (\delta_2 - \varepsilon_n)x_n + \delta_1 y_n - (\alpha - \varepsilon_n)z_n + w_n, \end{aligned} \tag{A.3}$$

which when written in matrix form gives a matrix with unit determinant. If the distribution $P_n(x_n, y_n, z_n, \omega_n)$ at the step n is known, then the analogous distribution at the step $(n + 1)$ is composed according to the rule

$$\begin{aligned} P_{n+1}(\tilde{x}_{n+1}, \tilde{y}_{n+1}, \tilde{z}_{n+1}, \tilde{w}_{n+1}) &= \int d\varepsilon_n dx_n dy_n dz_n dw_n \times \\ &\times P(\varepsilon_n)P_n(x_n, y_n, z_n, w_n)\delta\left(\tilde{x}_{n+1} - x_{n+1}\right) \times \\ &\times \delta\left(\tilde{y}_{n+1} - y_{n+1}\right)\delta\left(\tilde{z}_{n+1} - z_{n+1}\right)\delta\left(\tilde{w}_{n+1} - w_{n+1}\right), \end{aligned} \tag{A.4}$$

where x_{n+1}, y_{n+1}, z_{n+1}, ω_{n+1} are expressed through x_n, y_n, z_n, ω_n by formula (*A*.3). Let us inverse relation (*A*.3) and come to integration over x_{n+1}, y_{n+1}, z_{n+1}, ω_{n+1}; since the Jacobian is equal to unity and the δ-functions are trivially removed, we obtain

$$\begin{aligned} &P_{n+1}(x_{n+1},y_{n+1},z_{n+1},w_{n+1}) = \\ &= \int d\varepsilon_n P(\varepsilon_n) P_n(x_n,y_n,z_n,w_n), \end{aligned} \tag{A.5}$$

where x_n, y_n, z_n, ω_n are expressed through x_{n+1}, y_{n+1}, z_{n+1}, ω_{n+1} by the inverse of (*A*.3). Expanding over the deviations $x_{n+1}-x_n$, $y_{n+1}-y_n$, . . . and keeping the first order terms in α, Δ and the second order terms in ε, we get

$$\begin{aligned} \frac{\partial P}{\partial n} &= \alpha\left[y\frac{\partial P}{\partial x} - x\frac{\partial P}{\partial y} - w\frac{\partial P}{\partial z} + z\frac{\partial P}{\partial w}\right] - \\ &- \delta_1\left[z\frac{\partial P}{\partial x} + w\frac{\partial P}{\partial y} + x\frac{\partial P}{\partial z} + y\frac{\partial P}{\partial w}\right] + \\ &+ \delta_2\left[-w\frac{\partial P}{\partial x} + z\frac{\partial P}{\partial y} + y\frac{\partial P}{\partial z} - x\frac{\partial P}{\partial w}\right] + \\ &+ \frac{1}{2}\varepsilon^2(w-y)^2\left[\frac{\partial^2 P}{\partial x^2} + 2\frac{\partial^2 P}{\partial x\partial z} + \frac{\partial^2 P}{\partial z^2}\right] + \\ &+ \frac{1}{2}\varepsilon^2(x-z)^2\left[\frac{\partial^2 P}{\partial y^2} + 2\frac{\partial^2 P}{\partial y\partial w} + \frac{\partial^2 P}{\partial w^2}\right] + \\ &+ \varepsilon^2(x-z)(w-y)\left[\frac{\partial^2 P}{\partial x\partial y} + \frac{\partial^2 P}{\partial x\partial w} + \frac{\partial^2 P}{\partial z\partial y} + \frac{\partial^2 P}{\partial z\partial w}\right]. \end{aligned} \tag{A.6}$$

Introducing the polar coordinates

$$\begin{aligned} x &= r_1\cos\varphi, \quad y = r_1\sin\varphi, \\ z &= r_2\cos\theta, \quad w = r_2\sin\theta, \end{aligned} \tag{A.7}$$

we obtain

$$\begin{aligned} \frac{\partial P}{\partial n} &= \alpha\left[-P'_\varphi + P'_\theta\right] - \Delta\cos(\theta-\varphi-\beta)\left[r_2P'_{r_1} + r_1P'_{r_2}\right] + \\ &+ \Delta\sin(\theta-\varphi-\beta)\left[\frac{r_1}{r_2}P'_\theta - \frac{r_2}{r_1}P'_\varphi\right] + \\ &+ \frac{1}{2}\varepsilon^2\left\{\sin^2(\theta-\varphi)\left[r_2^2P''_{r_1r_1} + 2r_1r_2P''_{r_1r_2} + r_1^2P''_{r_2r_2}\right] + \right. \\ &+ 2\sin(\theta-\varphi)\left[r_1 - r_2\cos(\theta-\varphi)\right]\left[\frac{r_2}{r_1}P''_{r_1\varphi} + P''_{r_2\varphi} - \frac{r_2}{r_1^2}P'_\varphi\right] + \\ &+ 2\sin(\theta-\varphi)\left[r_1\cos(\theta-\varphi) - r_2\right]\left[\frac{r_1}{r_2}P''_{r_2\theta} + P''_{r_1\theta} - \frac{r_1}{r_2^2}P'_\theta\right] + \\ &+ \left[r_1 - r_2\cos(\theta-\varphi)\right]^2\left[\frac{1}{r_1^2}P''_{\varphi\varphi} + \frac{1}{r_1}P'_{r_1}\right] + \\ &+ \left[r_1\cos(\theta-\varphi) - r_2\right]^2\left[\frac{1}{r_2^2}P''_{\theta\theta} + \frac{1}{r_2}P'_{r_2}\right] + \\ &\left. + 2\left[r_1 - r_2\cos(\theta-\varphi)\right]\left[r_1\cos(\theta-\varphi) - r_2\right]\frac{1}{r_1r_2}P''_{\varphi\theta}\right\}. \end{aligned} \tag{A.8}$$

Now come from r_1, $r_2$to the variables ρ, ξ

$$r_1^2 + r_2^2 = 1 + 2\rho, \qquad r_1^2 - r_2^2 = \xi. \tag{A.9}$$

It is easy to check that all terms with derivatives over ξ disappear; hence the value of ξ remains constant during the evolution, and for physical reasons we can put $\xi = 1$. Then

$$r_1 = \sqrt{1+\rho}, \qquad r_2 = \sqrt{\rho} \tag{A.10}$$

in accordance with the canonical representation (2). In this case, the evolution equation will take the form

$$\begin{aligned} \frac{\partial P}{\partial n} &= \alpha\left[-P'_\varphi + P'_\theta\right] - \Delta\cos(\theta-\varphi-\beta)2r_1r_2P'_\rho + \\ &+ \Delta\sin(\theta-\varphi-\beta)\left[\frac{r_1}{r_2}P'_\theta - \frac{r_2}{r_1}P'_\varphi\right] + \\ &+ \frac{1}{2}\varepsilon^2\left\{4r_1^2r_2^2\sin^2(\theta-\varphi)P''_{\rho\rho} + \right. \\ &+ \left[2r_1^2 + 2r_2^2 - 4r_1r_2\cos(\theta-\varphi)\right]P'_\rho + \\ &+ 4r_2\sin(\theta-\varphi)\left[r_1 - r_2\cos(\theta-\varphi)\right]P''_{\rho\varphi} + \\ &+ 4r_1\sin(\theta-\varphi)\left[r_1\cos(\theta-\varphi) - r_2\right]P''_{\rho\theta} - \\ &- 2\sin(\theta-\varphi)\frac{r_2\left[r_1 - r_2\cos(\theta-\varphi)\right]}{r_1^2}P'_\varphi - \\ &- 2\sin(\theta-\varphi)\frac{r_1\left[r_1\cos(\theta-\varphi) - r_2\right]}{r_2^2}P'_\theta + \\ &+ \left[\frac{r_1 - r_2\cos(\theta-\varphi)}{r_1}\right]^2P''_{\varphi\varphi} + \left[\frac{r_1\cos(\theta-\varphi) - r_2}{r_2}\right]^2P''_{\theta\theta} + \\ &\left. + 2\left[\frac{r_1 - r_2\cos(\theta-\varphi)}{r_1}\right]\left[\frac{r_1\cos(\theta-\varphi) - r_2}{r_2}\right]P''_{\varphi\theta}\right\}. \end{aligned} \tag{A.11}$$

At substitutions (*A*.7) and (*A*.9) we did not renormalize the probability; however, as a result of two substitutions we have

$$\begin{aligned} &4P(x,y,z,w)dx\,dy\,dz\,dw = \\ &= P(\rho,\xi,\varphi,\theta)d\rho\,d\xi\,d\varphi\,d\theta, \end{aligned} \tag{A.12}$$

and the above renormalization is reduced to a constant multiplier, which is insignificant due to the linearity

of the evolution equation. Introducing the combined phases (3), we have

$$\begin{aligned}\frac{\partial P}{\partial n}&=2\alpha P'_{\psi}-\Delta\cos(\psi-\beta)2r_1r_2P'_{\rho}+\\ &+\Delta\sin(\psi-\beta)\left[\left(\frac{r_1}{r_2}+\frac{r_2}{r_1}\right)P'_{\psi}+\left(\frac{r_1}{r_2}-\frac{r_2}{r_1}\right)P'_{\chi}\right]+\\ &+\frac{1}{2}\varepsilon^2\left\{4r_1^2r_2^2\sin^2\psi P''_{\rho\rho}+\left[2r_1^2+2r_2^2-4r_1r_2\cos\psi\right]P'_{\rho}+\right.\\ &+4\sin\psi\left(r_1r_2-r_2^2\cos\psi\right)\left(-P''_{\rho\psi}+P''_{\rho\chi}\right)+\\ &+4\sin\psi\left(r_1^2\cos\psi-r_1r_2\right)\left(P''_{\rho\psi}+P''_{\rho\chi}\right)-\\ &-2\sin\psi\left(\frac{r_2}{r_1}-\frac{r_2^2}{r_1^2}\cos\psi\right)\left(-P'_{\psi}+P'_{\chi}\right)-\\ &-2\sin\psi\left(\frac{r_1^2}{r_2^2}\cos\psi-\frac{r_1}{r_2}\right)\left(P'_{\psi}+P'_{\chi}\right)+\\ &+\left(\frac{r_1-r_2\cos\psi}{r_1}\right)^2\left(P''_{\psi\psi}-2P''_{\psi\chi}+P''_{\chi\chi}\right)+\\ &+\left(\frac{r_1\cos\psi-r_2}{r_2}\right)^2\left(P''_{\psi\psi}+2P''_{\psi\chi}+P''_{\chi\chi}\right)+\\ &\left.+\left(\frac{r_1-r_2\cos\psi}{r_1}\right)\left(\frac{r_1\cos\psi-r_2}{r_2}\right)\left(-P''_{\psi\psi}+P''_{\chi\chi}\right)\right\}.\end{aligned}\tag{A.13}$$

Substituting (*A*.10) and transforming the right-hand side to the sum of full derivatives, we have the final evolution equation having the structure (4):

$$\begin{aligned}\frac{\partial P}{\partial n}&=\left\{-2\Delta\cos(\psi-\beta)\sqrt{\rho(1+\rho)}P+2\varepsilon^2\sin^2\psi\rho(1+\rho)P'_{\rho}+\right.\\ &+\varepsilon^2\left[(1-2\sin^2\psi)(1+2\rho)-2\cos\psi\sqrt{\rho(1+\rho)}\right]P+\\ &\left.+2\varepsilon^2\sin\psi\left[\cos\psi(1+2\rho)-2\sqrt{\rho(1+\rho)}\right]P'_{\psi}\right\}_{\rho}+\\ &+\left\{\left[2\alpha+R\Delta\sin(\psi-\beta)\right]P+\varepsilon^2\sin\psi(R-2\cos\psi)P+\right.\\ &\left.+\frac{1}{2}\varepsilon^2(2-R\cos\psi)^2P'_{\psi}\right\}_{\psi}+\\ &+\left\{\frac{\Delta\sin(\psi-\beta)+\varepsilon^2\sin\psi(1-R\cos\psi)}{\sqrt{\rho(1+\rho)}}P+\right.\\ &\left.+\frac{\varepsilon^2\cos\psi(R\cos\psi-2)}{\sqrt{\rho(1+\rho)}}P'_{\psi}+\frac{\varepsilon^2\cos^2\psi}{2\rho(1+\rho)}P'_{\chi}\right\}_{\chi}.\end{aligned}\tag{A.14}$$

Integration over χ leads to the evolution equation for $P(\rho,\psi)$ obtained in [16,17], and integration over ρ and ψ leads to equation (27) for $P(\chi)$.

REFERENCES

1. P. W. Anderson, D. J. Thouless, E. Abrahams, D. S. Fisher, *Phys. Rev. B* **22**, 3519 (1980).
2. R. Landauer, *IBM J. Res. Dev.* **1**, 2 (1957); *Phil. Mag.* **21**, 863 (1970).
3. V. I. Melnikov, *Sov. Phys. Sol. St.* **23**, 444 (1981).
4. A. A. Abrikosov, *Sol. St. Comm*. **37**, 997 (1981).
5. N. Kumar, *Phys. Rev. B* **31**, 5513 (1985).
6. B. Shapiro, *Phys. Rev. B* **34**, 4394 (1986).
7. P. Mello, *Phys. Rev. B* **35**, 1082 (1987).
8. B. Shapiro, *Phil. Mag.* **56**, 1031 (1987).
9. I. M. Lifshitz, S. A. Gredeskul, L. A. Pastur, *Introduction to the Theory of Disordered Systems*, Nauka, Moscow, 1982.
10. C. W. J. Beenakker, *Rev. Mod. Phys.* **69**, 731(1997).
11. X. Chang, X. Ma, M. Yepez, A. Z. Genack, P. A. Mello, *Phys. Rev. B* **96**, 180203 (2017).
12. L. I. Deych, D. Zaslavsky, A. A. Lisyansky, *Phys.Rev. Lett.* **81**, 5390 (1998).
13. L. I. Deych, A. A. Lisyansky, B. L Altshuler, *Phys. Rev. Lett.* **84**, 2678 (2000); *Phys. Rev. B* **64**, 224202 (2001).
14. L. I. Deych, M. V. Erementchouk, A. A. Lisyansky, *Phys. Rev. Lett.* **90**, 126601 (2001).
15. I. M. Suslov, *J. Exp. Theor. Phys.* **129**, 877 (2019) [*Zh. Eksp. Teor. Fiz.* **156**, 950 (2019)].
16. I. M. Suslov, *Phil. Mag. Lett.* **102**, 255 (2022).
17. I. M. Suslov, *J. Exp. Theor. Phys.* **135**, 726(2022) [Zh. Eksp. Teor. Fiz. **162**, 750 (2022)].
18. S. I. Bozhevolnyi, *I. M. Suslov*, *Phys. Scr.* **98**, 065024 (2023).
19. I. M. Suslov, *Adv. Theor. Comp. Phys.* **6**, 77 (2023).
20. N. F. Mott, E. A Davis, *Electron Processes in Non-Crystalline Materials*, Oxford, Clarendon Press, 1979.
21. V. V. Brazhkin, I. M. Suslov, *J. Phys. – Cond. Matt.* **32** (35), 35LT02 (2020).
22. I. M. Suslov, *J. Exp. Theor. Phys.* **131**, 793 (2020) [Zh. Eksp. Teor. Fiz. **158**, 911 (2020)].
23. S. John, *Phys. Rev. Lett.* **53**, 2169 (1984).
24. P. Van Albada, A. Lagendijk, *Phys. Rev. Lett.* **55**, 2692 (1985).
25. P. W. Anderson, *Philos. Mag. B* **52**, 505 (1985).
26. S. John, *Phys. Rev. Lett.* **58**, 2486 (1987).
27. S. I. Bozhevolnyi, V. S. Volkov, K. K. Leosson, *Phys. Rev. Lett.* **89**, 186801 (2002).
28. D. S. Wiersma, *Nature Photon*. **7**, 188 (2013).

29. Zh. Shi, M. Davy, A. Z. Genack, *Opt. Express* **23**, 12293 (2015).
30. W. H. Press, B. P. Flannery, S. A. Teukolsky, W. T. Wetterling, *Numerical Recipes in Fortran*, *Cambridge University Press*, 1992.
31. L. D. Landau, E. M. Lifshits, *Electrodynamics of Continuous Media*, *Oxford*, *Pergamon Press*,1984.
32. Ch. K. Kao, *Nobel Prize Lecture*, 2009.
33. D. W. Pohl, W. Denk, M. Lanz, *Appl. Phys. Lett.* **44**, 651 (1984).
34. D. W. Pohl, L. Novotny, *J. Vac. Sci. Technol. B* **12**, 1441 (1994).
35. A. L. Lereu, A. Passian, Ph. Dumas, *Int. J. Nanotechnol.* **9**, 488 (2012).
36. G. Binning, H. Rohrer, *Helv. Phys. Acta*. **55**, 726 (1982).
37. G. Binning, C. F. Quate, C. Gerber, *Phys. Rev. Lett.* **56**, 930 (1986).
38. E. Meyer, *Progress in Surface Science* **41**, 3 (1992).
39. S. I. Bozhevolnyi, V. A. Zenin, R. Malreanu, I. P. Radko, A. V. Lavrinenko, *Opt. Express* **24**, 4582 (2016).
40. I. M. Vellekoop and A. P. Mosk, *Phys. Rev. Lett.* **101**, 120601 (2008).
41. S. M. Popoff, G. Lerosey, R. Carminati, M. Fink, A. C. Boccara, and S. Gigan, *Phys. Rev. Lett.* **104**, 100601 (2010).